Contributions to Canadian Mineralogy, 1928

FROM THE
DEPARTMENT OF MINERALOGY AND PETROGRAPHY
UNIVERSITY OF TORONTO

THE UNIVERSITY OF TORONTO PRESS
1928

TABLE OF CONTENTS

THE CRYSTAL STRUCTURE OF SPERRYLITE

BY

G. AMINOFF AND A. L. PARSONS

Material used, Source, and Purification

The material used in this research consisted of crystals and crystal fragments from the Vermillion mine near Sudbury, Ontario, which were furnished by the Royal Ontario Museum of Mineralogy. Examination under the microscope showed that there was a transparent substance present. Treatment with methylene iodide failed to remove this material, so that it was supposed to be cassiterite, which is mentioned in the original description of sperrylite as one of the associated minerals.[1] This mineral was then removed by hand-picking under a binocular microscope so that the sperrylite was free from impurities. The purified sample was then ground in an agate mortar to an impalpable powder.

Apparatus, camera, etc.

The source of the X-rays was a Siegbahn-Hadding metal X-ray tube with an iron anticathode. The powder was exposed in two cameras, one with a 50 mm. diameter, the other with an 80 mm. diameter. In the latter the prepared powder was supported on a single silk-worm fibre. The thread with the powder did not exceed 0.1 mm. in diameter. This camera had been calibrated with an equally thin preparation of rock salt, and a curve was made for the $\sin^2\frac{\theta}{2}$ plotted against the distance measured on the film for the different lines. The figures thus obtained in the large camera were used for the calculation of the space lattice. For comparison, powder photograms of pyrite were made in both cameras inasmuch as a similar structure might be expected in both minerals. A new value for the cube edge of pyrite was calculated which is equal to 5.40Å. The powder photograms are shown in figures 1, sperrylite,

[1] Am. J. Sc., Ser. III, 37, pp. 67, 71.

and 2, pyrite. The sine squares, intensities and symbols for the powder photogram of sperrylite are shown in Table I, and for pyrite in Table II.

A small crystal of sperrylite .3×.35×.4 mm. was used to make a rotating photogram. A cube face was orientated perpendicular to the axis of rotation of the camera as described in an earlier paper by one of us (Aminoff).[2] The diameter of the camera was 56.8 mm. The symbols and intensities of the spots are listed in Table III.

Symmetry, Dimension of Lattice, and Number of Molecules in Unit Cube

According to the measurements made by Penfield,[3] Walker,[4] and Goldschmidt and Nicol,[5] sperrylite crystallizes in the pyritohedral class of the cubic system T_h. In the cubic system, all sine squares must be expressed as a constant multiplied by an integer. As a matter of fact, all sine squares which were calculated from the graph were in perfect agreement with this law.

The specific gravity of sperrylite was recently determined on pure material by Spencer[6] who obtained the value 10.603 by hydrostatic weighing and a corrected value $D_4^{19.5} = 10.58$.

From the equation

$$\sin^2\frac{\theta}{2} = \frac{\lambda^2}{4a^2}(H^2+K^2+L^2)$$

and by using measurements on the graph of lines with $\sin^2\frac{\theta}{2}$ up to .786 the value for the cube edge was calculated

for Feα 1.934 Å $\quad a = 6.022$ Å $\quad \frac{\lambda\alpha^2}{4a^2} = .02637$

Feβ 1.753 Å $\quad a = 5.961$ Å $\quad \frac{\lambda\beta^2}{4a^2} = .02167$

weighted average $a = 6.00$ Å

[2]Geol. För. Förh., 48, 38, 1926.
[3]Am. J. Sc., Ser. III, 38, 67, and Zs. Kr., 15, 290.
[4]Am. J. Sc., Ser. IV, 1, 110 and Zs. Kr., 25, 561.
[5]Am. J. Sc., Ser. IV, 15, 450, 1903.
[6]Min. Mag., XXI, 95, 1926.

TABLE I

POWDER PHOTOGRAM OF SPERRYLITE

Fe Radiation. Radius of Camera 40 mm.

No.	Intensity	mm.	$\sin^2\frac{\theta}{2}$ (obs.)	$\sin^2\frac{\theta}{2}$ (calc.)	*HKL* (α)	*HKL* (β)
1	m−	41.1	.063	.065		111
2	m+	45.4	.078	.079	111	
3	w	47.7	.087	.087		200
4	st.	52.7	.106	.105	200	
5	m	59.3	.133	.132	210	
6	m	65.0	.159	.158	211	
7	w	68.5	.173	.173		220
8	m+	76.1	.210	.211	220	
9	m	81.6	.238	.238		311
10	w−	85.5	.261	.260		222
11	st	90.9	.288	.290	311	
12	w	93.1	.303	.303		321
13	m	95.3	.316	.316	222	
14	w	99.9	.343	.343	320	
15	m−	104.2	.367	.369	321	
16	w−	111.2	.409	.412		331
17	w−	115.0	.434	.433		420
18	w−−	118.2	.452	.455		421
19	m	126.7	.502	.501	331	
20	m	129.9	.526	.527	420	
21	w	134.0	.552	.554	421	
22	w−	138.5	.582	.585		511
23	w	139.5	.588	.580	332	
24	m	147.1	.633	.633	422	
25	w−−	157.5	.692	.693		440
26	st	160.6	.712	.712	511	
27	m−	170.2	.768	.765	520	
28	w−	173.2	.786	.780		600
29	w−	175.2	.796	.791	521	
30	st	186.3	.844	.844	440	
31	w	192.0	.869	.871	522	
32	st	205.7	.920	.923	531 α_1	
33	m	206.1	.922		531 α_2	
34	st	213.3	.945	.949	600 α_1	
35	m	215.3	.950		600 α_2	

TABLE II

POWDER PHOTOGRAM OF PYRITE

Fe Radiation. Radius of Camera 40 mm.

No.	Intensity	mm.	$\sin^2\frac{\theta}{2}$ (obs.)	$\sin^2\frac{\theta}{2}$ (calc.)	*HKL* (α)	*HKL* (β)
1	w	50.0	.095	.096	111	
2	w	53.0	.107	.106		200
3	st	58.5	.130	.129	200	
4	st	65.6	.161	.161	210	
5	m	72.3	.191	.192	211	
6	w−	76.2	.210	.210		220
7	m	84.7	.256	.254	220	
8	w	90.8	.291	.290		311
9	st	101.2	.350	.352	311	
10	w	106.6	.383	.385	222	
11	w	111.8	.415	.417	320	
12	m	117.1	.448	.448	321	
13	w	142.8	.606	.608	331	
14	w	148.0	.638	.640	420	
15	w	153.5	.669	.672	421	
16	w−	159.5	.705	.705	332	
17	w	170.7	.772	.769	422	
18	w−	174.0	.792	.790		521
19	st	190.6	.863	.864	511	
20	st	207.2	.926	.927	520	
21	st	218.0	.964	.961	521	

TABLE III

ROTATING PHOTOGRAM OF SPERRYLITE

Fe α Radiation. Radius of Camera 28.4 mm.

Equator. $L=0$								
Forms.....	200	210	220	320	420	520	440	
Intensity...	m	w−	st	w	st	w−	st	
First row. $L=1$								
Forms.....	111	211	311	321	331	421	511	521
Intensity...	m−	m−	st	w	m	w	st	w
Second row. $L=2$								
Forms.....	102	112	202	222	302	402	422	522
Intensity...	w	w−	m	m	w	m	st	m

NOTE.—On the equatorial line the planes 200, 420, 440, and 620 gave reflections for Fe.β radiation.

From measurements on the rotating photogram the length of the cube edge was also calculated.

First row of spots $a=5.88$ Å
Second row of spots $a=5.92$ Å
Average $a=5.90$ Å

This determination shows that the value of the cube edge which was determined from the powder photogram for the cube edge is the correct one. As the radius of the camera for the powder photogram is larger than that of the camera for the rotating photogram, and as the diameter of the preparation in the first camera was much less, the value obtained from the powder photogram must be considered to be more nearly accurate.[7]

From the equation

$$10^{-24}\times a^3\times S.G.=N(PtAs_2)\times 1.65\times 10^{-24}$$
$$N=4.02.$$

If we assume that there are four molecules in the unit cube, the specific gravity calculated from the same equation is 10.59.

Point Group and Position of Atoms

As there are reflections from planes which contain both odd and even indices, the lattice cannot be face-centred. In like manner as there are faces, the sum of whose indices is an odd number, the lattice cannot be body-centred. The lattice is therefore the simple cubic lattice and the only possible point groups are T_h^1, T_h^2, and T_h^6.

As the unit cell contains 4 molecules of $PtAs_2$, and there are no chemical reasons why the platinum atoms should not be alike, and the arsenic atoms also alike, we must find for the platinum atoms a four-fold position and for the arsenic atoms an eight-fold position.[8]

[7] Ramsdell obtained a value of 5.94 Å for the cubic edge of sperrylite. Am. Min., 10, 202.

[8] If instead of pyritohedral hemimorphism we assume tetratohedrism (T) we must consider point groups T^1 and T^4, but as these cannot have eight equivalent atoms they are eliminated from further consideration.

As there is no four-fold position in T_h^1 we have to consider only T_h^2 and T_h^6. There is a medium strong line from 210, a weak one from 320, and a medium to weak one from 520. As the structure factors for 210, 320, and 520 in T_h^2 are zero, the only remaining space group is T_h^6 in which reflections from these forms are possible.

In T_h^6 there is only one eight-fold position possible, the 8*h* which has the co-ordinates (see Wyckoff's tables).

$$uuu:\ u+\tfrac{1}{2},\ \tfrac{1}{2}-u,\ \bar{u}:\ \bar{u},\ u+\tfrac{1}{2},\ \tfrac{1}{2}-u:\ \tfrac{1}{2}-u,\ \bar{u},\ u+\tfrac{1}{2}$$
$$\bar{u}\bar{u}\bar{u}:\ \tfrac{1}{2}-u,\ u+\tfrac{1}{2},\ u:\ u,\ \tfrac{1}{2}-u,\ u+\tfrac{1}{2}:\ u+\tfrac{1}{2},\ u,\ \tfrac{1}{2}-u.$$

The arsenic atoms must have these positions which are the same as those for sulphur in pyrite.

For the platinum atoms there are two possibilities, 4*b* and 4*c* (Wyckoff). The co-ordinates of these positions are:

$$4b\quad 000:\ \tfrac{1}{2}\tfrac{1}{2}0:\ \tfrac{1}{2}0\tfrac{1}{2}:\ 0\tfrac{1}{2}\tfrac{1}{2}.$$
$$4c\quad \tfrac{1}{2}\tfrac{1}{2}\tfrac{1}{2}:\ \tfrac{1}{2}00:\ 0\tfrac{1}{2}0:\ 00\tfrac{1}{2}.$$

The combination of 4*b* with 8*h* and 4*c* with 8*h* give in reality the same structure, depending on the value given to *u*.

Summary

Sperrylite has a simple cubic lattice. The length of the cube edge is 6.00 Å. There are four molecules in the unit cube. Position of the atoms, *Pt.* 4*b*, *As* 8*h*. This type of structure is the same as that found in pyrite. The value 5.40 Å was determined for the cube edge of pyrite.

Stockholm, June 20, 1927.

A NEW TELLURIDE OCCURRENCE IN QUEBEC

By ELLIS THOMSON

Telluride ores have already been noted in the province of Quebec, in the vicinity of Opasatika Lake,[1] where the telluride mineral is variously described as petzite or sylvanite; but minerals carrying tellurium, at least as recorded up to date, are not so prevalent as in the sister province of Ontario. The exploitation of the copper and zinc ores of the Rouyn area, however, has opened up a new field of mineral investigation, and new localities for rare minerals are being discovered from year to year.

Through the kindness of Mr. Hugh Park, Manager of the Nipissing Mines, Limited, the writer was fortunate in procuring for the Royal Ontario Museum of Mineralogy some wonderful specimens of telluride ore, from a new locality in Montbray township in the province of Quebec, which were obtained from the Robb-Montbray property, situated about three miles northwest of the southeast corner of that township. They were taken from a point in the mine workings about 150 feet from the surface in a raise from the second level. The seven specimens submitted to the writer for microscopic determination varied in size from 2″×1″ ×¾″ to 1″×1″×¾″.

Small bits were separated from the seven specimens mentioned above and carefully polished for microscopic examination. Most of these polished sections were set in holders of sealing wax, being too small to be handled successfully for the grinding and polishing operations. In all, ten of these sections were prepared, so that none of the minerals present in the ore might be overlooked. The determinations were carried out with the aid of microchemical and physical tests, and the tellurium was determined qualitatively by the

[1]Cairnes, D. D. Jour. Can. Min. Inst., 1911, p. 190, p. 200; Harvie, Robt., Jr. Jour. Can. Min. Inst., 1911, p. 166.

sulphuric acid reaction. In all the sections examined the telluride minerals predominated over all others, making this one of the most striking telluride occurrences ever found in Canada. Some of the larger specimens were studded also with native gold, giving them a most spectacular aspect. The ores are of two types, which are sufficiently different to deserve separate mention. As a description of each specimen would necessarily involve considerable repetition, these two types will be described in some detail as though from but two specimens, while in reality representing a composite picture of several.

Type 1

In this type the predominating minerals are tetradymite, altaite, and chalcopyrite, but smaller amounts of sphalerite, pyrrhotite, gold, krennerite, petzite, pyrite, and chalcocite are also present. The tetradymite and altaite occur in very intimate association, with the latter following the basal cleavage planes of the former to produce a pseudo-eutectic structure (Plate II, Fig. 1). The intimate physical and chemical relations so common to certain lead and bismuth minerals, notably galena and matildite, are here repeated very faithfully. This structure may have originated in any one of three ways. The altaite may have been deposited somewhat later than the tetradymite, following the cleavage planes as convenient channels; it may have been deposited contemporaneously; or it may be a case of a former solid solution of the two constituents with ex-solution of the minor one as temperature and pressure decreased. The similarity between this structure and other structures noted in the case of ilmenite and magnetite, orthoclase and albite in perthite, and in certain steels, and attributed to the phenomenon of ex-solution, is noteworthy. A still more striking parallel, in appearance at least, is to be found in the micrographic intergrowth of quartz and feldspar known as micropegmatite. In one or two of the sections examined the native gold seems to form a third member of this intergrowth. Of the remaining associated minerals pyrite seems to have been the first and

chalcocite the latest to form. The sphalerite is associated chiefly with the chalcopyrite (Plate II, Fig. 2) and follows in some cases the parting directions in that mineral, while the pyrrhotite is in the form of irregular masses and is associated either with chalcopyrite or with the tellurides (Plate II, Fig. 3). Petzite usually follows the boundary lines of the other tellurides (Plate II, Fig. 3), as does the native gold in some instances (Plate II, Fig. 4). Coloradoite is present in but one of the ten specimens and in very small amounts. It shows the same relations as to mineral association as the petzite. Pyrite is present in the form of a few small isolated crystals cut in places by the altaite. Chalcocite occurs as an alteration product of the chalcopyrite and follows convenient boundaries between that mineral and others (Plate II, Fig. 5).

The order of genetic succession in the specimens of this type appears to be as follows: Pyrite, chalcopyrite and pyrrhotite, sphalerite, krennerite, tetradymite and altaite, petzite and coloradoite, native gold, and chalcocite.

Type 2

In this type of ore, krennerite is the predominant constituent, pyrite and chalcopyrite are present in considerable quantities, while minor amounts of native gold, altaite, tetradymite, petzite, sphalerite, pyrrhotite and chalcocite also occur. Krennerite has a brilliant lustre and shows a good basal cleavage. It is most intimately associated with pyrite and chalcopyrite and resembles the former in colour. Altaite and tetradymite are found in the same form as in Type 1, though present in much smaller amount, the native gold in association chiefly with the krennerite. The other minor constituents have much the same relations as in Type 1. Pyrite is present in crystal form, the crystals showing an octahedral habit. Chalcopyrite is associated with all the other minerals and sometimes appears as a thin coating on the pyrite crystals. In other places one or two crystals of chalcopyrite of sphenoidal habit are seen to be covered with

a thin black layer of chalcocite. This kind of alteration, as in the specimens of Type 1 is common, however, to all the chalcopyrite whether crystallized or massive. The order of deposition is the same as for Type 1, but with the quantitative proportions of the different minerals varying considerably from those in that part of the ore.

These two types of telluride ore grade into one another and at times lead to an almost bewildering variety of minerals. In one small section, about 10 mm.×14 mm., no less than eleven minerals were observed, five of them tellurides. The gangue mineral in both types is translucent quartz of medium grain, but in the specimens examined it is present in very small amount. Though no new minerals are recorded, the extraordinary richness of occurrence of these rare minerals seemed to justify this short description. The tellurides occur localized in a comparatively small pocket, but it is to be hoped that further investigation will reveal more of this valuable material. The writer is greatly indebted to the Nipissing Mines, Limited, and to their general manager, Mr. Hugh Park, for providing a sufficient number of specimens to allow of a thorough examination.

PLEOCHROIC HALOES IN BIOTITE

BY

D. E. KERR-LAWSON

In a previous paper on haloes,[1] the writer described in some detail uranium haloes in a biotite from near Murray Bay, Quebec. These haloes in the Murray Bay mica were examined in unusually thin sections, including less than one-tenth of the halo diameter, whereas halo sections examined by Joly[2] are said by him to have included from one-third to one-quarter of the halo diameter. Among other features it was pointed out that the Murray Bay haloes, examined in the exceptionally thin sections referred to, were distinctly made up of five rings, whereas the uranium haloes examined by Joly were stated by him to have shown only four. Moreover, micrometer measurements indicated that the innermost of these five rings corresponded pretty closely in position with what was to be expected from the air range of Uranium I. In other words, although probably of great antiquity, these haloes did not seem to show the anomaly found by Joly in old haloes, on the basis of which he suggested that uranium formerly disintegrated faster than it now does. The present article presupposes an acquaintance with the former one, and is an account of the continuation of the work therein described.

Since the former work was published the writer has continued the study of the Murray Bay and other haloes, devoting his attention more particularly to the utility of the micro-photometer in determining the space distribution

[1]Kerr-Lawson, D. E. Univ. of Toronto Studies, Geol. Series No. 24, 1927, p. 54.

[2]Joly, J. Phil. Trans. Roy. Soc. London, Series A, Vol. 17, 1916-18, p. 55. Joly, J., and Rutherford, E. Phil. Mag., April, 1913.

of the darkening effect in them. A curve obtained from a preliminary trial of the machine in this connection was reproduced in the earlier article, and although it was too imperfect to be of much value, yet it held out promise of interesting results, if sufficiently perfect material, and sufficiently good photomicrographs, could be obtained. Chiefly as a consequence of the development of this method, results are now available, which, it is hoped, are of sufficient interest to merit publication, both as confirming the conclusions previously reached, and as perhaps throwing some new light on the nature of the formation of haloes in biotite.

In the earlier work, the method used for determining the distribution of the darkening effect in the halo consisted simply in the measurement of the radii of the several dark rings by means of a micrometer microscope. This was the method used by Joly, and although if carried out with suitable equipment and with careful attention to the lighting, it will give good results up to a certain point, nevertheless it is subject to some serious and inevitable limitations. No *quantitative* comparative information can be obtained regarding the intensity of the darkening at different points; the boundary between a dark ring and the adjacent lighter region may appear more or less transitional (especially with high magnification), and must be selected to a certain extent by the judgment of the observer; and, finally, difficulty may be experienced in seeing clearly the detail in the dark central portion of the halo, with the surrounding field brightly illuminated.

By using the micro-photometer a curve is obtained giving the light absorption as ordinates, and the distance from the centre of the halo as abscissae. The dark rings are represented as maxima on the curve. The procedure consisted in photographing the halo to a linear magnification of 400, giving an image on the negative about two and one-half centimetres in diameter. With an image of this size it was possible to indicate accurately, by means of marks on the plate, on opposite sides of the negative image and well away from it, the diameter along which the absorption was to be

determined. The negative was then placed in the micro-photometer in such a way that the line indicated would be traversed. Two examples of actual curves obtained in this manner are shown in Fig. 1. The position of the axis of ordinates, which corresponds to the centre of the halo, can be determined from the fact that this line must divide symmetrically the horizontal distribution of the curve. If, then, we assume (*a*) that the outer limit of the darkening

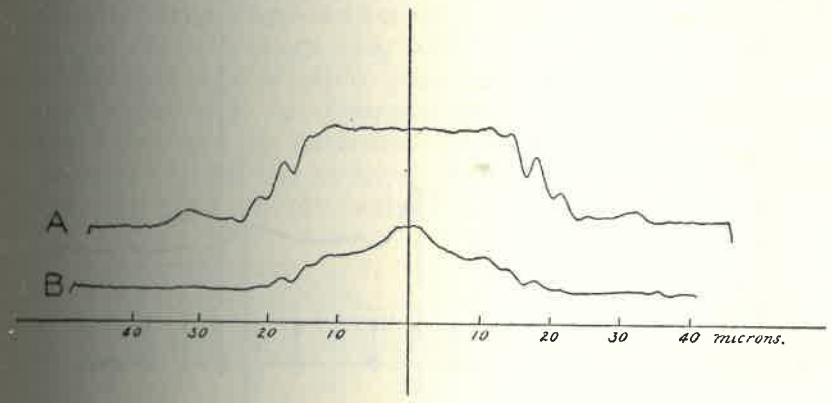

Fig. 1

effect in mica corresponds to the "end of the range" of *RaC* particles in air, and (*b*) that the ratio $\frac{\text{Range in Air}}{\text{Range in Mica}}$ is nearly the same for the other alpha particles, as it is for those from *RaC*, then by marking off this outer limit of the darkening (seen on the curve as the point where it drops down to the level representing the unaffected mica) as 7.0 cm., we obtain a scale of abscissae whereby we may compare the radius of any feature of the halo in mica directly with equivalent alpha particle penetration of air.

Fig. 2 shows a tracing of one-half of one of the micro-photometer curves, together with such a scale. It will be noted that the maximum representing the inner ring is not significantly displaced from the point at about 2.2 cm.,

where, according to Joly[1], the ring due to Uranium I[2] should occur.

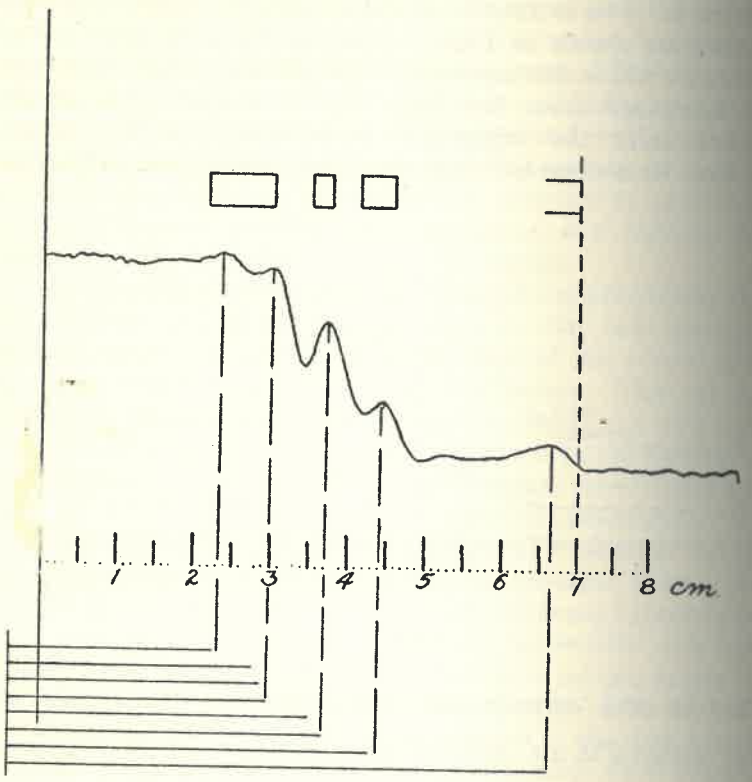

Fig. 2

The occurrence of five rings in the uranium halo, as shown in the writer's photomicrographs both in this (Plate III, Fig. 2) and in the former article, and recorded in the five maxima on the micro-photometer curves, is in much better agreement

[1]Joly, J., Phil. Trans. Roy. Soc. Lon., *loc. cit.*, p. 76.

[2]Recent determinations of the ranges of the alpha particle involved have yielded somewhat different values from those accepted at the time of Joly's paper. The changes, however, are not such as to affect the point referred to. See page 19.

with the values of the air ranges of alpha particles from the U-series than is the occurrence of four. From an inspection of the outer part of the light absorption curve (between 5 cm. and 7 cm. in Fig. 2) it is evident that divergent homogeneous alpha radiations from *RaC* do not cause in mica, in this part of their range, any effect which is sufficiently sharply accentuated at a definite distance from the centre, to distinguish them from another set of alpha particles having nearly the same range. Hence, two or more sets of alpha particles whose ranges are not very different, may be expected to give rise to a single ring only. Fig. 3 shows the ranges of the eight sets of alpha particles ejected by uranium in equilibrium with its disintegration products, plotted one above the other as horizontal lines, all measured off from the same vertical line as zero. It is apparent that although there are eight discrete values for these ranges, the eight

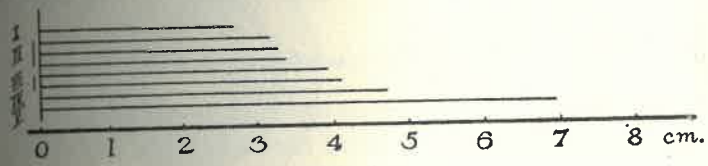

Fig. 3

nevertheless fall into five groups. We have, first, Uranium I; then Ionium, Uranium II, and Radium, very close together; then Radium F and Radon, very close together; then Radium A; and finally Radium C.

Ranges of α Particles

Uranium I	2.70	Lawrence, Trans. Nova Scotia Institute, 1927.
Uranium I	3.28	
Ionium	3.194	Geiger, Zeit. f. Physik, VIII, 1921, p. 45.
Radium	3.389	
Radon	4.122	
Radium A	4.722	
Radium C	6.971	
Radium F	3.925	

Moreover, if we make the reasonable assumption that the maxima on the micro-photometer curve represent the regions of maximum darkening activity of the alpha particles which cause them, and that this maximum darkening activity occurs at the same distance from the end of the range, for all the alpha particles, then it becomes apparent, from an inspection of Fig. 2, that the spatial distribution of the five rings is in very good agreement with the distribution of the ranges of the five groups of alpha particle when these ranges are plotted according to the scale in the same figure.

Above the curve in Fig. 2 are plotted the positions of the four rings according to Joly. It may be seen from this that the region occupied by his inner ring is occupied in the material under discussion by two rings, and the writer is

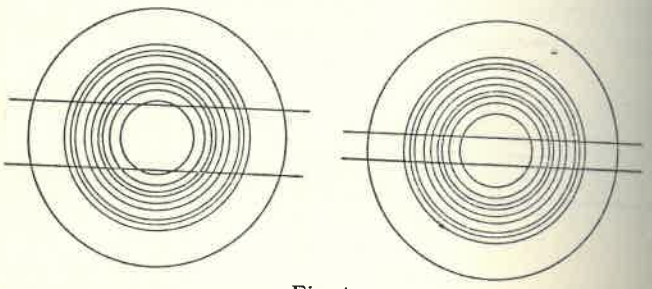

Fig. 4

satisfied that in this material, at any rate, it would be impossible to resolve these two rings in sections as thick as those used by Professor Joly.

It is interesting in this connection to compare, by means of a drawing, the relation of the halo to the thick and thin sections. Fig. 4, above, shows the portion of the halo included in the thinnest sections mentioned by Professor Joly (A), compared with the portion included in the thickest sections used by the writer (B). It is evident that in the case the inner rings there is in (A) a very pronounced overlap due to the sphericity of the halo, and this is the very portion where Joly found the anomaly. In the case of the thorium haloes, for which he secured a satisfactory agreement through-

out, the two inner rings were much farther apart[1], so that the question of overlap would not be expected to have so much effect.

The probability that the Murray Bay haloes are old geologically, and hence such as might be expected to show the Joly anomaly to a pronounced degree, if it existed, is indicated not only by the fact of their occurrence in rocks regarded as Precambrian, but also by the very small size of the nuclei which have given rise to them. The evidence that the nuclei were later in origin than the mica introduces an element of uncertainty, but Joly's haloes showed equally definite evidence of this, and while admitting their later origin, he attributed it to the action of mineralizing solutions immediately following the crystallization of the magma, in which case they would, of course, be essentially contemporaneous with the containing rock.

Nature of the Process of Halo Formation

Joly[2] seems to be the only writer who has hitherto analysed in detail the considerations involved in the process of formation of radioactive haloes in biotite. It is proposed, first of all, to give a brief statement of his conclusions regarding them, and secondly, to discuss some consequences of the writer's observations.

Joly observed a certain analogy between radioactive darkening in a mica and alpha particle ionization in a gas. The distribution of the darkening in the halo seemed to suggest this, and it seemed not improbable that the darkening effect on the mica molecules might vary along the path of the alpha particle in much the same way as the ionizing effect on gas molecules. If this were the case, then the relative distribution of the darkening effect in the mica should be the same as the relative distribution of intensity of ionization produced by the same active nucleus in a gas.

Fig. 5 is a curve showing the variation of ionization with

[1]Joly, J., Phil. Trans. Roy. Soc. London, *loc. cit.*, p. 68.
[2]Joly, J., Phil. Trans. Roy. Soc. Lon., *loc. cit.*, p. 53 *et seq.*

distance from the source, for homogeneous parallel alpha radiations from *RaC*, having a range of 7.0 cm. in air at 15 deg. C. and 760 mm. pressure. In the uranium haloes, however, we are dealing with uranium in equilibrium with its disintegration products, and hence not with homogeneous alpha radiation, but with rays from the same source having eight different ranges. Referring to Fig. 5, if in addition to the alpha particles from *RaC*, coming to rest at 7.0 c.m., we had another set of particles coming to rest at 4.7 cm., then to obtain a curve giving the composite ionization for the two sets acting together, the curve is slid along the axis of abscissae until it intersects the latter at 4.7 cm. instead of at 7.0 cm. The ordinates in its new position are then added

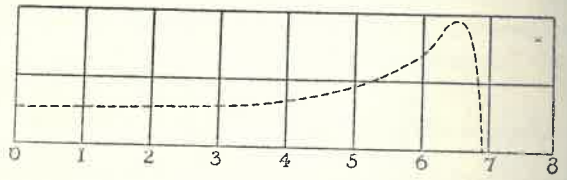

Fig. 5

to the coincident ordinates in the former position, and the new ordinates thus obtained are those of the required composite curve. Such a curve was obtained experimentally by Bragg for radium and its disintegration products. By this method Joly built up the composite ionization curve for the eight alpha rayers of the uranium series, present in equilibrium quantities in the source. This is reproduced in Fig. 6 (see footnote No. 2, p. 18).

This curve, however, applies only to parallel radiations. In the halo the particles diverge from a common centre, so that correction must be made for the operation of the inverse square law. Joly applied this correction, and obtained the curve in Fig. 7. The effect of this correction is practically to wipe out all the bends in the curve except the minimum at about 5 cm., and the maximum at about 6.5 cm., due to *RaC*. As the distribution of the darkening in the halo

showed a marked concentric arrangement with several alternating shells of darker and lighter material, Joly concluded that this distribution conformed more closely to the curve for parallel radiations than to the corrected curve. He accounted for this by supposing that the higher velocity alpha particles, in traversing the regions darkened by those of lower velocity, reversed the darkening effect of the latter.

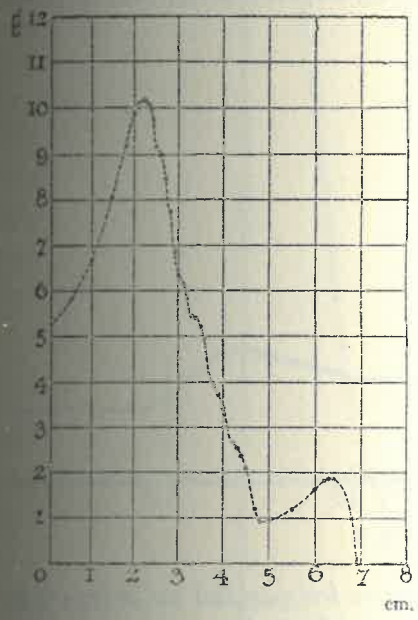

Fig. 6

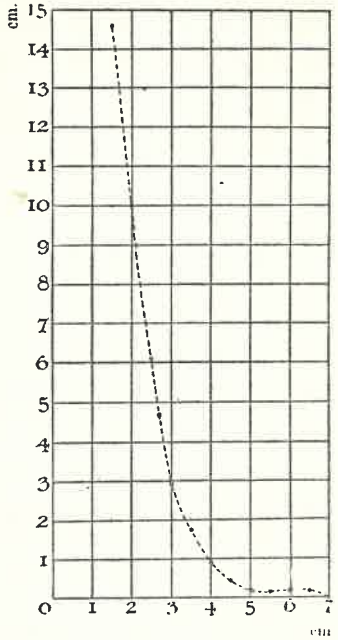

Fig. 7

He indicated that such a reversal effect might be expected to fall off very rapidly as the distance from the centre increased, and hence might be expected to counteract more or less the operation of the inverse square law. He also instanced the known cases of the reversal of the effects of light stimuli in photography as being somewhat analogous phenomena.

On account of their continuously quantitative character

the micro-photometer curves should be well adapted to throw some light on these questions. In a portion of the curves, representing the two-sevenths of the halo radius most remote from the centre, we can see the darkening effect, along the latter part of their range, of the divergent homogeneous alpha radiations from *RaC*, independent of other radiations. In Fig. 8, which is a reproduction of this portion of the curve, the part between the dotted lines, proceeding from left to right, first descends, then rises again, and finally falls off to the level of the unaltered mica.

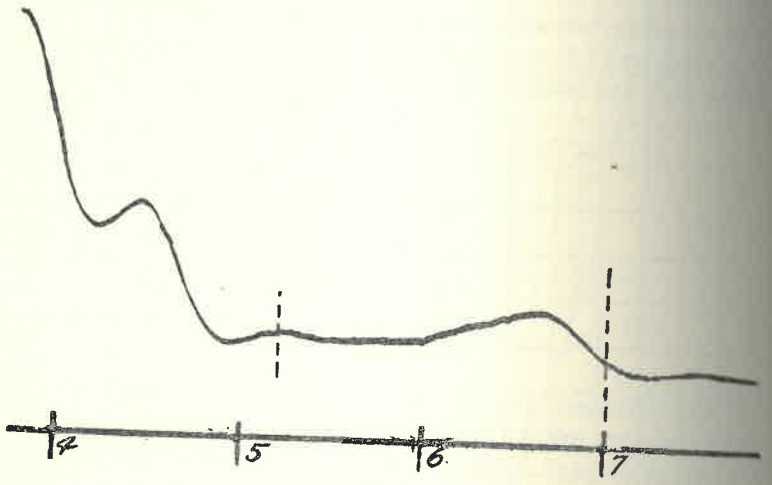

Fig. 8

If the Geiger ionization curve for parallel radiations from *RaC* (Fig. 5) be replotted in such a way as to take into account the divergence of the radiations in the halo, a curve of the form shown in Fig. 9 is obtained. If this curve were to be cut off at approximately 5 cm. by a depression connected with the set of alpha particles of next longest range (*RaA*), then the remaining (outer) portion of it would be of the same form as that part of the actual micro-photometer curve between the dotted lines in Fig. 8. The relation and significance of the depression referred to will appear later.

Reference was made in the writer's former paper to the

peculiar effects observed where two haloes overlap, and photo micrographs were reproduced there illustrating these effects. A further photo micrograph showing the phenomenon is reproduced in Plate IV, Fig. 1. The remarkable feature is that where one of the light inter-annular regions of one halo coincides with a normally dark ring of another, the coincident

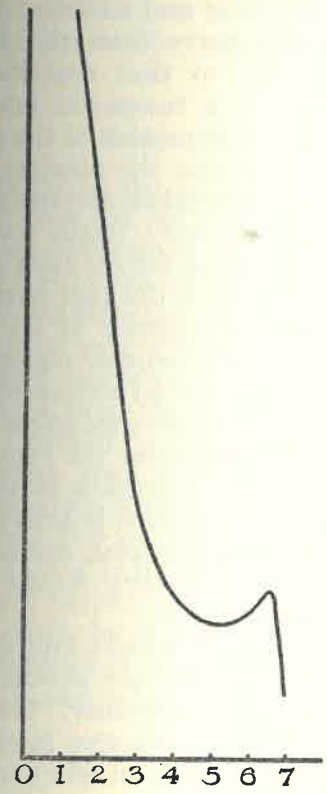

Fig. 9

region is lighter than is the dark ring away from the area of overlap. As these inter-annular regions are themselves positively darkened with respect to the unaffected mica, a fact which is established by the micro-photometer curves, it inevitably follows that, in these regions in the halo, effects

from different radiations are not only not additive darkening, but must be in part subtractive.

Looking back at the micro-photometer curve in Fig. 2, if we suppose the part of the curve due to *RaC* alone to be extrapolated backwards without sharp bends, and if the effects of the several lots of alpha particles which cause the halo were wholly darkening and additive, we should be able to build up the entire curve from the *RaC* curve by an additive process similar to that described in connection with the building up of a composite ionization curve for several alpha rayers. An inspection of the actual form of the curve will serve to show that the maxima corresponding to the dark rings, and the depressions corresponding to the inter-annular regions, are relatively much too contrasted and accentuated to be accounted for by such a process. These considerations, together with the fact that the overlapping haloes show indisputable evidence of an inhibition of the darkening effect in the inter-annular regions, lead the writer to conclude that the pronounced concentric structure in the haloes is preserved, not by a reversal effect falling off rapidly and more or less uniformly from the centre outwards, and thereby counteracting the operation of the inverse square law, but by a reversal effect which is active at the end of the range of each set of alpha particles, presumably about that region on their path where they would cease to darken previously non-darkened biotite.

If this were the case one should find evidence of such a terminal reversal effect around the extreme outer periphery of one halo, where it overlaps another. Owing to the greatly reduced density of radiation effective in this portion of the halo one would not expect such an effect to be very marked. Nevertheless, the writer observed several apparent instances of it, and in one case was able to secure photographic confirmation of it (Plate IV, Fig. 2).

Referring back to the two micro-photometer curves reproduced in Fig. 1, A represents a curve from a rather well-darkened halo (Plate III, Fig. 1), while B was obtained from a halo in a less advanced state (Plate III, Fig. 2). It will be noted that in B we have some suggestion of the rapid falling off of intensity of darkening with distance from the centre, which is to be expected in the inner part of the halo from the operation of the inverse square law. In B, however, the top of the curve is more or less flat, and a comparison of the two suggests very strongly that the darkening effect on the mica builds up to a maximum, which is naturally reached first at the centre, and to which the rest of the halo is gradually brought.

Conclusion

In his former paper on the subject, the writer stated that the Murray Bay haloes did not seem to show any anomaly with regard to the determined constants of the uranium series. The work herein described decidedly confirms this, and shows also that the structure of the haloes agrees (subject to inherent limitations) very well with the determined ranges of the alpha particles concerned. In so far as they may be comparatively judged from the literature the haloes appear to be exceptionally perfect in definition for their kind; and in the writer's opinion, they afford absolutely no suggestion that different disintegration constants prevailed during their formation from those now accepted.

The persistence of a marked concentric distribution of the darkening effect in the haloes is apparently due to a terminal reversal effect, by which, in the region of the end of the range of a given set of alpha particles, the development of darkening due to other sets of alpha particles is inhibited.

EXPLANATION OF PLATES

Plate I, Fig. 1—Powder photogram of sperrylite. Fe. radiation. Radius of camera 40 mm.

Plate I, Fig. 2—Powder photogram of pyrite. Fe. radiation. Radius of camera 40 mm.

Plate II, Fig. 1—Dark grey = altaite, light grey = tetradymite, etched with dilute HCl, × 112.

Plate II, Fig. 2—s = spalerite, ch = chalcopyrite, a = altaite, t = tetradymite, pr = pyrrhotite, pe = petzite, ×112.

Plate II, Fig. 3—pe = petzite, kr = krennerite, a = altaite, t = tetradymite, pr = pyrrhotite, ×112.

Plate II, Fig. 4—g = gold, a = altaite, ch = chalcopyrite, kr = krennerite, ×112.

Plate II, Fig. 5—cc = chalcocite, ch = chalcopyrite, kr = krennerite, pe = petzite, pr = pyrrhotite, ×112.

Plate III, Fig. 1—Photomicrograph of halo from which micro-photometer curve "A" was obtained. (×800.)

Plate III, Fig. 2—Photomicrograph of halo from which micro-photometer curve "B" was obtained. (×800.)

Plate IV, Fig. 1—Photomicrograph of overlapping haloes. (×800.)

Plate IV, Fig. 2—Photomicrograph of overlapping haloes showing terminal reversal effect due to *RaC* around periphery. (×800.)

Plate I

Figure 1

Figure 2

Figure 1

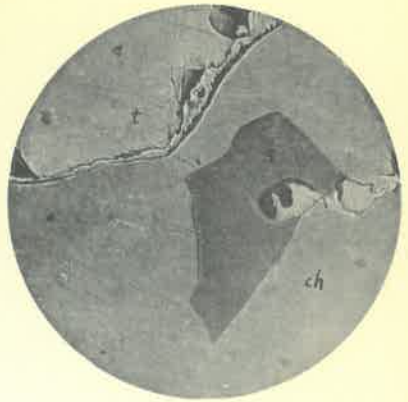

Figure 2

Figure 3

Figure 4

Figure 5

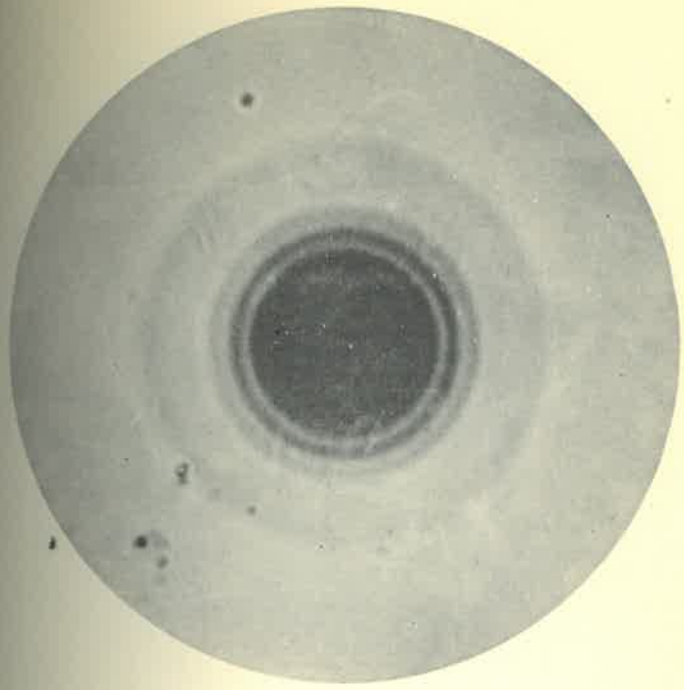

Figure 1

Figure 2

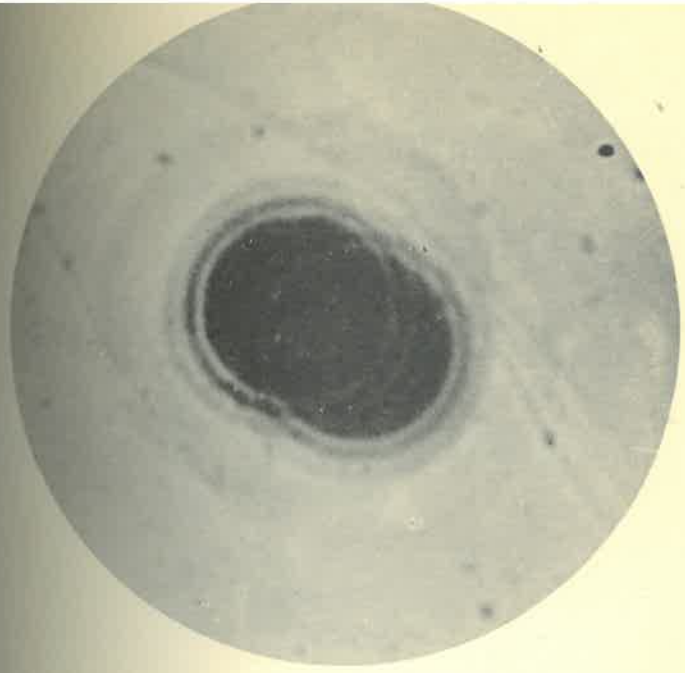

Figure 1

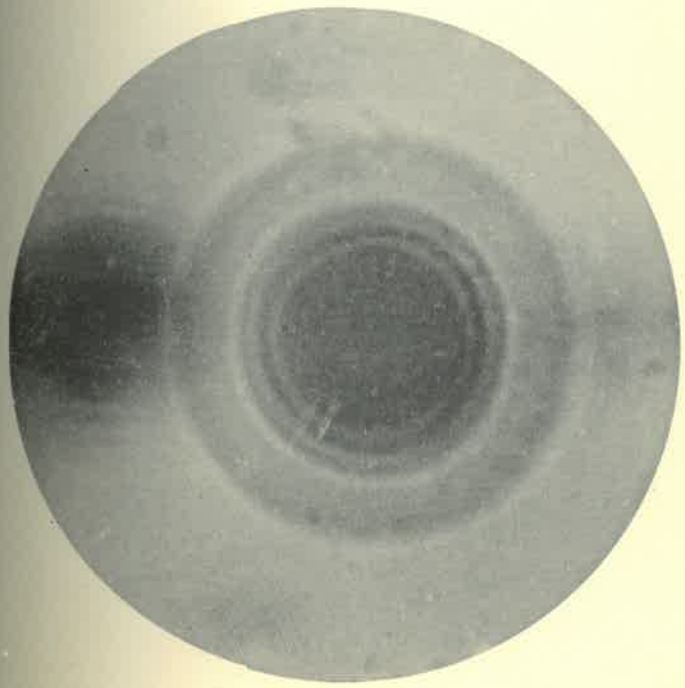

Figure 2